



In situ template generation of silver nanoparticles as amplification tags for ultrasensitive surface plasmon resonance biosensing of microRNA

Xin Wang, Ting Hou, Haiyang Lin, Wenxin Lv, Haiyin Li^{*,*}, Feng Li^{*}

College of Chemistry and Pharmaceutical Sciences, Qingdao Agricultural University, Qingdao, 266109, People's Republic of China

ARTICLE INFO

Keywords:

Silver nanoparticles
Surface plasmon resonance
In situ generation
Amplification tags
miRNA

ABSTRACT

Surface plasmon resonance (SPR) biosensing strategies have drawn substantial attention due to their advantages of label free, real time, and high performance, but complicated modification procedures and strict reaction conditions of amplification tags associated with current SPR biosensors hinder their potential utilizations. Herein, an in situ prepared AgNPs-based SPR biosensor for MicroRNA (miRNA) sensitive detection was developed based on hybridization chain reaction (HCR) without the biomodification on amplification tags. The target miRNA initiated the HCR of the hairpin probes to generate long double strand DNA (dsDNA) chains that were immobilized on SPR disk. Thus, with Ag⁺ intercalating into dsDNA chains, large numbers of AgNPs generated after NaBH₄ reduction, resulting in the significantly elevated SPR angle. Further, the SPR angle is positively proportional to target miRNA concentrations. As a result, the in situ generated AgNPs-based SPR biosensor realized exceptional let-7a detection with linear range of 0.001–0.1 pM and detection limit (LOD) of 0.35 fM, lower than that of other SPR biosensors that used modifiable amplification tags. Featured with the modification-free characteristic and excellent performance, the proposed strategy provides new way for ultrasensitive detection of miRNA, and allows to detect other biomarkers by simply verifying the target responsive substances, and thus has a great potential for health and early disease diagnosis.

1. Introduction

MicroRNAs (miRNAs), as endogenous and non-coding RNAs, can selectively bind to messenger RNAs to regulate the gene expression, and have been proved to be closely relevant with cancer, neurodegeneration, hepatitis, and other diseases (Causa et al., 2015; Plotnikova et al., 2014; Yan et al., 2017). In view of this, it is highly desirable to propose sensitive miRNAs strategies for disease diagnosis and treatment (Kelnar et al., 2014; Li et al., 2018a). Nevertheless, their small size, easy degradation, sequence homology, and low expression level make miRNAs sensitive quantitation disadvantageous using traditional techniques (Li et al., 2018b). From this context, novel techniques for miRNAs sensitive detection is in eager need (Chang et al., 2019; Ki et al., 2017; Masud et al., 2017; Park and Yeo, 2014). Among them, surface plasmon resonance (SPR) technique has drawn much more research attention due to the intrinsic features of real time, label free, and high sensitivity (Nguyen et al., 2015; Zeng et al., 2014; Zhou et al., 2018). For example, Thierry et al. realized the ultrasensitive SPR detection of miRNA based on an antibody conjugated gold nanoparticles (Yang et al., 2017). Lou et al. reported an ultrasensitive SPR PrP^{Sc} assay through using magnetic

nanoparticle as signal amplification tag (Lou et al., 2017). Despite the enhanced sensing performance, the aforementioned SPR biosensors all needed the modification on the amplification tags surface using biomolecules (Gandhiraman et al., 2011; Kobori et al., 2004; Li et al., 2017a; Wolf et al., 2005; Zubritsky, 2000), which was subject to some problems: 1) the modification procedures are time-consuming, complex, and costly; 2) the modification procedures and the steric hindrance of amplification tags may deactivate the immobilized molecules; 3) the reaction conditions are restrict, and easily make the amplification tags agglomerated (Qian et al., 2018; Wang et al., 2016; Li et al., 2017b). For the sake of addressing the issues above, we, herein, developed a novel SPR biosensor for miRNA ultrasensitive biosensing without the need to modify the amplification tags surface with biomolecules.

Recently, more and more evidences have demonstrated that the application of deoxyribonucleic acids (DNA) as templates is one of the most effective tools available for in situ generation of metal nanoparticles (Chen et al., 2012; Mehrgardi and Ahangar, 2011; Yang et al., 2015). Phosphate and amino groups are abundant in DNA, and contributed to binding to metal ions (Ag⁺, Pd²⁺, Cu²⁺, etc) with high

^{*} Corresponding author.

^{**} Corresponding author.

E-mail address: lifeng@qau.edu.cn (F. Li).

affinity (Cunningham et al., 2015; Lin et al., 2011a; Luo et al., 2015; Ma et al., 2017; Tian et al., 2010; Zhou et al., 2017a). These binding metal ions could be reduced to metal nanoparticles along with the dsDNA skeletons (Yang et al., 2015; Zhou et al., 2017b), which have been widely applied in sensitive analysis of L-cysteine (Lin et al., 2011b), carcino-embryonic antigen (CEA) (Zhou et al., 2017a), Cyclin-D1 (Zhou et al., 2017b), and miRNAs (Xia et al., 2014; Yang et al., 2015). For example, using DNA templates, in situ prepared Pd nanoparticles were applied in development of electrochemical biosensor for sensitive detection of CEA (Zhou et al., 2017a); in situ prepared Ag nanoparticles were utilized to develop fluorescent biosensor for sensitive detection of biothiols (Chen et al., 2012). Besides, these metal nanoparticles were reported to enjoy high refractive index (Liu et al., 2015, 2017), which make for the SPR angle effectively increasing. Taking account of these fascinating properties, we have reasons to believe that in situ template formation strategy appears to be the best candidate for developing ultrasensitive SPR biosensor that avoids the biomolecules modification on amplification tags surface. Unfortunately, as far as we are considered, using DNA templates, in situ prepared metal nanoparticles have not been applied in SPR assays to amplify the signal.

Herein, we developed an in situ prepared Ag nanoparticles (AgNPs)-based SPR biosensor for ultrasensitive detection of miRNA based on target-initiated hybridization chain reaction (HCR). AgNPs have high real part and low imaginary part in dielectric constants (Meng et al., 2018; Ocsoy et al., 2013), and thus would significantly increase the SPR angle when they were immobilized on SPR disk. HCR is one of the most commonly used amplification techniques (Li et al., 2012, 2018b; Yao et al., 2015), and can achieve the improved sensing performance via the formation of large amounts of dsDNA. In addition, it can be carried out under mild conditions and does not need any enzymes. So, it is very interesting to realize SPR signal amplification via the combination of HCR and AgNPs. In this strategy, three DNA probes (ON1, ON2, and ON3) were elaborately designed so that they could capture target miRNA and subsequently the HCR was triggered to generate substantial dsDNA on the SPR disk. Moreover, in-depth researches have suggested that long dsDNA were favorable for in situ template generation of AgNPs compared with short ssDNA/dsDNA. If target miRNA is absent, ON2 and ON3 co-existed in the reaction solution, with only few dsDNA linked to SPR disk, and thus hardly any AgNPs generated along with the DNA skeletons, subsequently leading to small SPR angle change. The response of the DNA probes to target miRNA autonomously triggers the HCR to generate a long chain of dsDNA immobilized on SPR disk. As a result, with Ag^+ intercalating into the dsDNA, large amounts of AgNPs generated, resulting in the increased SPR angle. Further, the SPR angle is positively proportional to target miRNA concentrations. Therefore, the in situ prepared AgNPs-based SPR biosensor for miRNA sensitive biosensing was realized in the light of the increased SPR angle. This strategy combines the SPR biosensing, in situ template formation, with HCR-assisted signal amplification to get the miRNA biosensing with high sensitivity and good selectivity, and has a great potential for health and early disease diagnosis.

2. Experimental

2.1. Modification of the SPR disk

The SPR disk was put in the mixed solution (30% $\text{NH}_3\cdot\text{H}_2\text{O}$ /30% $\text{H}_2\text{O}_2/\text{H}_2\text{O}$) at 100 °C for 10 min to complete the cleaning procedure. After being washed with ultrapure water three times, the SPR disk was dried with N_2 . Prior to modification on SPR disk, ON1 was heated to 95 °C for 5 min, and then cooled down to 25 °C at a slow rate to ensure the generation of hairpin structure. Firstly, the SPR disk was put into 1.0 μM ON1 solution, and reacted for 12 h at 25 °C to fabricate ON1 modified SPR disk (ON1/Au) through the formation of Au–S bond. After rinsing with PBS, ON1/Au was put into 1.0 mM MCH solution for 1.0 h. Thus, the MCH/ON1/Au, which could recognize target miRNA, was

prepared and saved for the following experiment.

2.2. In situ prepared AgNPs-amplified SPR detection of miRNA

Both ON2 and ON3 transformed into the hairpin structure according to the thermal procedure of ON1 before application. For SPR detection, the MCH/ON1/Au was firstly installed on the SPR spectrometer. Then, 500 μL solution containing miRNA was injected into the flow cell, and miRNA hybridized with ON1 for 1.5 h to produce miRNA@ON1 complex. Then miRNA/MCH/ON1/Au generated and was washed with ultrapure water. Further, 500 μL solution containing ON2 (0.5 μM) and ON3 (0.5 μM) was pumped into the reaction chamber and incubated for 1.5 h to complete the HCR and form long dsDNA chains (ON3 + ON2/miRNA/MCH/ON1/Au). After that, 500 μL AgNO_3 solution was added into the chamber and reacted with ON3 + ON2/miRNA/MCH/ON1/Au for 0.5 h to finish the intercalation. Finally, a 500 μL freshly prepared NaBH_4 solution was injected and reacted for 1.5 h to reduce Ag^+ into AgNPs on SPR disk. For all steps, SPR spectra between angle and time were recorded.

3. Results and discussion

3.1. Principle of in situ template prepared AgNPs-based SPR biosensor

The schematic representation of the designed SPR biosensor based on in situ template generation of AgNPs and HCR to assist signal amplification for miRNA ultrasensitive biosensing is shown in Fig. 1. In our work, the sequences of DNA probes (ON1, ON2 and ON3) are elaborately designed. Each DNA probe exhibits a single electrophoresis band without other secondary structure (Fig. 2A), justifying their distinguished stability. For gel electrophoresis characterization, ON1-1, the sequences of which were the same as ON1, was used to replace ON1 for avoiding the influence of HS groups. ON1 contains the sequences complementary to target miRNA and oligonucleotide fragments embedded in the stem of ON2. ON2 and ON3 can hybridize with each other due to their complementary sequences in the presence of target miRNA. Firstly, probe ON1 was immobilized on SPR disk via the formation of Au–S bonds, and MCH was used as blocking agent to form a mixed monolayer to avoid any nonspecific adsorption (Bo et al., 2018; Hassani et al., 2018). In the absence of target miRNA, probes ON1, ON2 and ON3 maintained their hairpin structures unchanged, respectively. As expected, there are no newly appearing electrophoresis bands when they were mixed together in the absence of target miRNA (Fig. 2A). From this context, HCR could not be triggered to generate dsDNA accompanied with few Ag^+ intercalating in ON1, subsequently resulting in few AgNPs deposited on SPR disk. Thus, negligible SPR angle shift was determined. However, upon the addition of target miRNA, the following HCR was successfully driven. First of all, target miRNA disclosed ON1 to form miRNA@ON1 complex through the competitive hybridization reaction, which could be verified by the newly appearing band located at lower distance than that of ON1. After that, the exposed purple fragment in ON1 hybridized with orange segment in ON2 via complementary base pairing to unfold ON2. As such, the violent fragment in ON2 was activated to unfold ON3 to release pink domain, the sequences of which in turn hybridized with orange and yellow segment in another ON2 to expose violent fragment. At this rate, target miRNA would trigger the HCR to generate abundant dsDNA, which were confirmed by the gel electrophoresis information that new band appeared at the lowest distance. Moreover, upon the formation of duplex DNA, multiple Ag^+ intercalated into dsDNA chains (Zhou et al., 2017b). With the help of NaBH_4 reduction, abundant AgNPs formed and deposited on SPR disk, thus contributing to a hugely increased SPR signal. Using this “signal-on” SPR biosensor, highly sensitive detection of miRNA would be achieved.

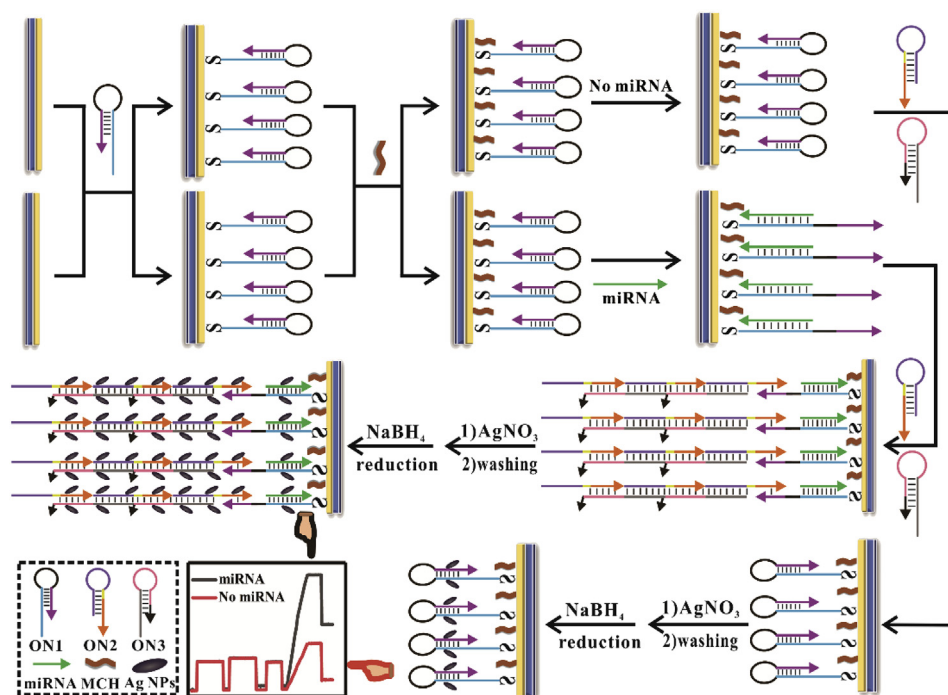


Fig. 1. Schematic representation of in situ DNA template prepared AgNPs-based SPR biosensor based on HCR for miRNA ultrasensitive biosensing.

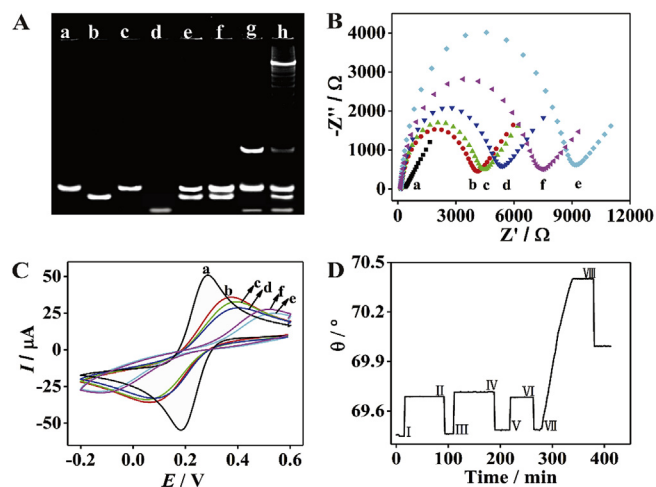


Fig. 2. (A) Nondenaturing PAGE analysis of different samples: (a) ON1-1, (b) ON2, (c) ON3, (d) let-7a, (e) ON2+ON3, (f) ON1-1+ON2+ON3, (g) ON1-1+let-7a, (h) ON1-1+let-7a+ON2+ON3. (B) Nyquist spectra and (C) CV curves of the different SPR disks in 5.0 mM $[K_3Fe(CN)_6]/[K_4Fe(CN)_6]$ solution: (a) Au, (b) ON1/Au, (c) MCH/ON1/Au, (d) let-7a/MCH/ON1/Au, (e) ON3+ON2/let-7a/MCH/ON1/Au, (f) AgNPs/ON3+ON2/let-7a/MCH/ON1/Au. (D) SPR angle (θ) of MCH/ON1/Au under different conditions versus the reaction time: (I) injecting in let-7a solution, (II) injecting in water, (III) injecting in solution containing ON2 and ON3 (0.5 μ M), (IV) injecting in water, (V) injecting in $AgNO_3$ solution (100 μ M), (VI) injecting in water, (VII) injecting in $NaBH_4$ solution (500 μ M), (VIII) injecting in water.

3.2. Electrochemical/SPR characterizations

To characterize the stepwise fabrication process of the established SPR biosensor, electrochemical impedance spectroscopy (EIS) was first conducted by using $[K_3Fe(CN)_6]/[K_4Fe(CN)_6]$ as indicator and the impedance spectra were shown in Fig. 2B. For the bare gold disk, the impedance spectrum suggested a relatively small electron transfer resistance (R_{et}) of $\sim 376.4 \Omega$, validating its high conductivity. After ON1 was self-assembled onto the SPR disk, a noticeable increase in R_{et} was

observed with value of $\sim 4100.1 \Omega$, implying the successful conjugation of SH-DNA on SPR disk. Accordingly, MCH modification made R_{et} increase to 4459.2 Ω . Upon the hybridization with target miRNA, the R_{et} increased to $\sim 5325.4 \Omega$. After the target-initiated HCR of ON2 and ON3, abundant dsDNA were immobilized on SPR disk when compared with that of miRNA/MCH/ON1/Au. Consequently, it was rational to get much higher R_{et} (9142.2 Ω) after HCR because of the enhanced electrostatic repulsion between $[K_3Fe(CN)_6]/[K_4Fe(CN)_6]$ and ON3+ON2/miRNA/MCH/ON1/Au (Mills et al., 2018). Nevertheless, the R_{et} value reduced obviously when AgNPs deposited on SPR disk, justifying the effective deposition of AgNPs along with the DNA skeletons. There is no denying that the decreased R_{et} was ascribed to AgNPs' high conductivity, which not only quickens the electron transfer, but also strengthens the response efficiency. The corresponding fabrication process could also be confirmed by cyclic voltammetry (CV) characterizations and the results were illustrated in Fig. 2C. The bare SPR disk gave a couple of reversible redox peaks located at 0.28 V and 0.18 V with high current. Nevertheless, the peak current reduced, respectively, along with the sequential modification of ON1/MCH/miRNA/ON2+ON3, powerfully proving their immobilizations on SPR disk. Owing to the in situ template generation of AgNPs and AgNPs-mediated conductivity enhancement, the current increased when AgNPs formed on the SPR disk.

To further confirm the modification procedures, SPR measurements of SPR disk at different stages were carried out (Fig. 2D). Upon the addition of target let-7a into the reaction system (stage I) and with the subsequently rinsing with water (stage II), the SPR angle increased negligibly compared with that of MCH/ON1/Au. After that, with ON2 and ON3 mixed solution being injected into SPR equipment, the SPR angle elevated from 69.45° to 69.49° , which was attributable to the successful immobilization of HCR products on SPR disk. When Ag^+ intercalated in HCR products, negligible increase in SPR angle was detected compared with that of ON3+ON2/let-7a/MCH/ON1/Au. Obvious increase in SPR angle was obtained once $NaBH_4$ solution was pumped, successfully indicating that AgNPs were formed and deposited on SPR disk.

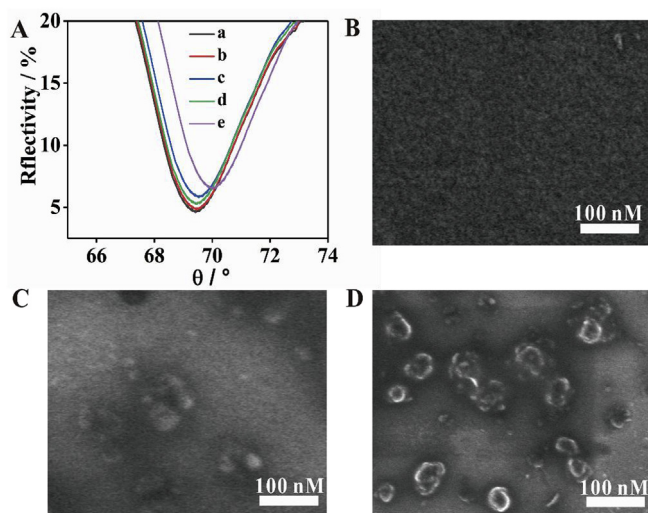


Fig. 3. (A) SPR responses under different conditions: (a) MCH/ON1/Au, (b) in the absence of target let-7a with HCR triggered, (c) in the absence of target let-7a with HCR triggered and AgNPs formed, (d) in the presence of target let-7a with HCR triggered, (e) in the presence of target let-7a with HCR triggered and AgNPs formed. SEM images of SPR disk (B), AgNPs/ON3+ON2/let-7a (0.1 pM)/MCH/ON1/Au (C), and AgNPs/ON3+ON2/let-7a (1.0 pM)/MCH/ON1/Au (D).

3.3. Feasibility investigation of in situ template prepared AgNPs-based SPR biosensor

To confirm the feasibility of the designed SPR biosensor based on in situ generation of AgNPs and HCR for miRNA assay, different SPR responses were obtained in the absence/presence of miRNA, using let-7a as the model target. As shown in Fig. 3A, compared with the SPR angle of MCH/ON1/Au (θ_0 , 69.45°), the ON3+ON2/let-7a/MCH/ON1/Au showed a small increase with the $\Delta\theta$ ($\Delta\theta = \theta_{\text{let-7a}} - \theta_0$, where $\theta_{\text{let-7a}}$ is the angle of the SPR disk under different let-7a concentrations) of only 0.04° . Thanks to the intercalation of Ag^+ in dsDNA chains (Chen et al., 2012; Lin et al., 2011b; Yang et al., 2015), massive AgNPs deposited on SPR disk with the aid of NaBH_4 and made the SPR angle increase to 69.99° with $\Delta\theta$ of 0.54° , which was greater than the variation of the sensing system in the absence of AgNPs. In addition, the AgNPs/ON3+ON2/let-7a/MCH/ON1/Au enjoyed excellent stability. The $\Delta\theta$ value changed slightly when they were stored for 5.0 days (Fig. S1). On the basis of the experimental results, it can be concluded the let-7a could truly enhance the SPR angle through target-initiated HCR, and more importantly, in situ template generated AgNPs could enhance the SPR angle more significantly. This obvious enhancement was attributed to the fact that AgNPs on SPR disk would evidently change the modified disk's reflectivity. So, it is completely feasible to use in situ template prepared AgNPs as amplification tags for improving the SPR angle. Nevertheless, in the absence of target let-7a, HCR could not be triggered, subsequently hampering Ag^+ to be immobilized on SPR disk. Thus, only few AgNPs were formed, leading to slight SPR angle shift. These SPR information apparently suggested that in situ prepared AgNPs-based SPR biosensor could achieve signal amplification and enhance the let-7a sensing performance.

Meanwhile, scanning electron microscopy (SEM) was employed to further explore the feasibility of the proposed SPR biosensor for let-7a biosensing. In contrast with the SEM image of bare gold disk (Fig. 3B), a small amount of nanoparticles with average diameter of 40 nm were acquired (Fig. 3C) in that of AgNPs/ON3+ON2/let-7a(0.1 pM)/MCH/ON1/Au. Undisputedly, the nanoparticles were deemed as the AgNPs that were synthesized and immobilized on SPR disk. However, when let-7a concentration increased, more amount of nanoparticles were determined from the SEM characterization (Fig. 3D), which implied

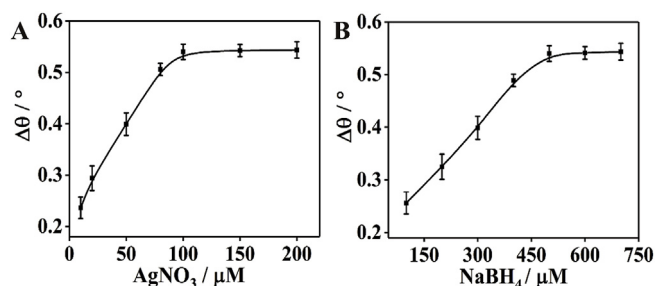


Fig. 4. The relationship between $\Delta\theta$ values and AgNO_3 (A)/ NaBH_4 (B) concentrations. Error bars represent the standard deviations of three repeated measurements.

that more dsDNA generated through let-7a-initiated HCR, subsequently resulting in more amount of AgNPs being deposited on SPR disk.

3.4. Optimization of experimental conditions

As mentioned above, dsDNA, which formed on SPR disk through the HCR of ON2 and ON3, are favorable for intercalating Ag^+ and depositing AgNPs on SPR disk. To guarantee the excellent performance of the established SPR biosensor, adequate amount of ON2 and ON3 are needed for generating dsDNA in this study. So, $0.5 \mu\text{M}$ was chosen as the optimal concentration for them. Further, the concentrations of AgNO_3 and NaBH_4 were optimized due to their direct influence on AgNPs generation. As manifested in Fig. 4A, the $\Delta\theta$ values increased progressively with AgNO_3 concentration elevating from 10 to $200 \mu\text{M}$, and whereas, with AgNO_3 concentrations higher than $100 \mu\text{M}$ the $\Delta\theta$ value hardly changed. The reason for this could be ascribed to the saturated intercalation of Ag^+ in dsDNA chains. Thus, $100 \mu\text{M}$ was chosen as the optimized AgNO_3 concentration. Accordingly, $500 \mu\text{M}$ was applied as the best amount for NaBH_4 from Fig. 4B and used in the whole experiment.

3.5. Analytical performance of in situ template prepared AgNPs-based SPR biosensor

To evaluate the sensing ability of our established SPR biosensor, the solution containing target let-7a with different amounts was injected into the SPR instrument under the best conditions and the SPR signals were showed in Fig. 5A and B. After the treatment with target let-7a solution, the SPR angle intensified significantly and is highly relied on the concentrations of let-7a. It came as no surprise to us that more let-7a impelled the preparation of more HCR products and intensified AgNPs formation, subsequently increasing the SPR angle. To qualitatively investigate the analytical performance, standard working curve between SPR angle shift ($\Delta\theta$) and let-7a concentrations ($C_{\text{let-7a}}$) was plotted (Fig. 5C). The $\Delta\theta$ was linearly proportional to $C_{\text{let-7a}}$ in the range from 0.001 to 0.1 pM, with regression equation of $\Delta\theta = 3.6191(C_{\text{let-7a}}/\text{pM}) + 0.2003$, correlation coefficient of 0.9886 and detection limit of 0.35 fM at 3σ . The comparison results of this proposed SPR biosensor with other methods were present in Tables S–2. It can be clearly found that such proposed SPR biosensor provided an ultralow LOD, which is lower than that of other existing SPR techniques that applied modified metal nanoparticles and magnetic nanoparticles as amplification tags. This ultrahigh sensitivity might be ascribed to the fact that in situ template formation strategy could immobilize larger numbers of amplification tags on SPR disk than modification strategy.

3.6. Selectivity of let-7a assay

Selectivity, as one of the essential factors in developing biosensor with excellent performance, was investigated by choosing five interferences (let-7b, let-7d, let-7k, miRNA-21, miRNA-429) as the target

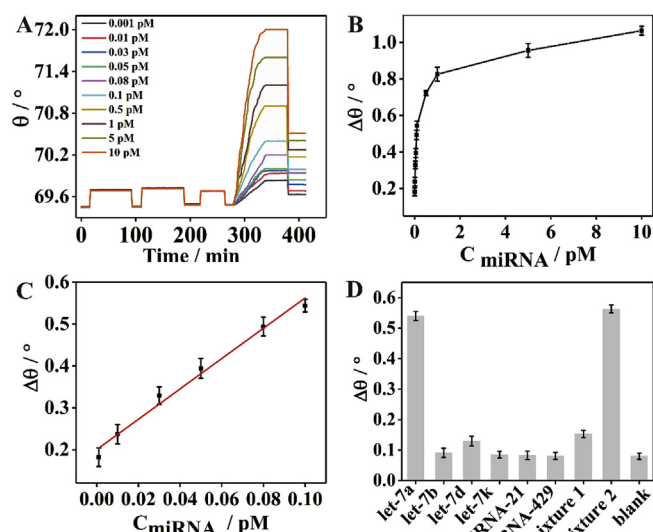


Fig. 5. (A) The responses of SPR angle to different let-7a concentrations in the range of 0.001–10 pM. (B) The relationship between $\Delta\theta$ and $C_{\text{let-7a}}$. (C) The linear standard curve for $\Delta\theta$ and $C_{\text{let-7a}}$. (D) Selectivity experiment of the established SPR biosensor subject to different miRNAs. The concentrations of all miRNAs were 0.1 pM. “Mixture 1” indicates the condition in the presence of let-7b, let-7d, let-7k, miRNA-21, and miRNA-429; “Mixture 2” indicates the condition in the presence of all miRNA; “blank” indicates the condition in the absence of let-7a. Error bars represent the standard deviations of three repeated measurements.

analytes instead of let-7a, respectively. These biomolecules belong to miRNAs family and have sequences similar to that of let-7a. For the precise evaluation, the SPR biosensor was subjected to them under the same conditions with that of let-7a and the experimental results were illustrated in Fig. 5D. Only in the presence of let-7a, the angle of the SPR biosensor exhibited a relatively significant change because of the good selectivity of hybridization reaction. Whereas the $\Delta\theta$ values in let-7b/let-7d/let-7k/miRNA-21/miRNA-429 solution, and even their mixing solution, were similar to that of the sample in the absence of target let-7a, and changed negligibly. This indicated that the $\Delta\theta$ is intensified through the target-activated hybridization reaction. Furthermore, these five miRNAs made little influence on the recognition efficiency and responsive ability of the established SPR biosensor toward let-7a. In brief, these information fully verified that the proposed strategy has the competence to discriminate let-7a against other miRNAs.

3.7. Application of the SPR biosensor in real sample

To test the practicability of the developed SPR biosensor, we carried out a series of recovery experiments through spiking different amount of let-7a into PBS-human serum mixing solution (V:V, 1:1). As illustrated in Table 1, for let-7a with different amount of 0.0050, 0.0200, 0.0500, and 0.0800 pM, the recoveries were determined to be 104.0%,

Table 1

Real sample analysis of in situ template prepared AgNPs-based SPR biosensor for let-7a spiked in diluted human serum.

Sample No.	Added (pM)	Mean measured (pM)	Mean recovery ^a (%)	RSD (%)
1	0.0050	0.0052	104.0	3.76
2	0.0200	0.0195	97.5	2.69
3	0.0500	0.0514	102.8	2.37
4	0.0800	0.0762	95.3	4.18

^a Recovery (%) = $100 \times (C_{\text{mean measured}}/C_{\text{added}})$.

97.5%, 102.8%, and 95.3%, respectively, with all RSDs lower than 4.5%, justifying the strong anti-interference ability and excellent reproducibility. Further, the developed SPR biosensor was used to determine let-7a in breast cancer patient's serum via the standard addition method (Fig. S2). The serum was diluted with PBS buffer until let-7a concentration was in the linear range of the established SPR biosensor. From the experimental results, the concentration of let-7a in serum was calculated to be 20.08 nM, which is in good agreement with that obtained from qRT-PCR method (21.26 nM). These data obviously validated that the in situ prepared AgNPs-based SPR biosensor offers great potential to achieve miRNA ultrasensitive detection in biological sample.

4. Conclusions

In summary, a novel SPR biosensor for let-7a ultrasensitive biosensing was successfully developed based on in situ template generation of AgNPs and AgNPs-mediated signal amplification strategies. The AgNPs were prepared in situ along with the target-initiated HCR products for avoiding the complex biomodification. Because of AgNPs' high refractive index, significantly increased SPR angle was determined. By coupling the HCR and in situ prepared AgNPs, the developed SPR biosensor provide sufficient sensitivity to detect let-7a with the detection limit of 0.35 fM, which is lower than that of other reported SPR methods that used modifiable amplification tags. In addition, it also exhibited effective discrimination ability between let-7a and other miRNAs. Taking advantages of high sensitivity and good selectivity, the application of the proposed biosensor in human serum samples was conducted with excellent reliability. Furthermore, this study demonstrated that in situ generation of metal nanoparticles may be an appropriate strategy for future development of novel SPR biosensor without the need to modify amplification tags with biomolecules. Therefore, we infer that this work would broaden and deepen the application perspective of SPR biosensor for biomolecules ultrasensitive biosensing.

Declaration of interests

The authors declare that they have no known competing financial interests or personal relationships that could have appeared to influence the work reported in this paper.

CRedit authorship contribution statement

Xin Wang: Conceptualization, Data curation, Investigation, Methodology, Writing - original draft. **Ting Hou:** Conceptualization, Investigation, Methodology, Resources. **Haiyang Lin:** Conceptualization, Data curation, Investigation, Methodology. **Wenxin Lv:** Conceptualization, Data curation, Investigation, Methodology. **Haiyin Li:** Conceptualization, Project administration, Software, Supervision, Resources, Writing - review & editing. **Feng Li:** Funding acquisition, Project administration, Resources.

Acknowledgements

This work was funded by the National Natural Science Foundation of China (21605093, 21775082, and 21675095), and the Special Foundation for Distinguished Taishan Scholar of Shandong Province (ts201511052).

Appendix A. Supplementary data

Supplementary data to this article can be found online at <https://doi.org/10.1016/j.bios.2019.05.006>.

References

- Bo, B., Zhang, T., Jiang, Y., Cui, H., Miao, P., 2018. *Anal. Chem.* 90 (3), 2395–2400.
- Causa, F., Aliberti, A., Cusano, A.M., Battista, E., Netti, P.A., 2015. *J. Am. Chem. Soc.* 137 (5), 1758–1761.
- Chang, J., Wang, X., Wang, J., Li, H., Li, F., 2019. *Anal. Chem.* 91 (5), 3604–3610.
- Chen, Z., Lin, Y., Zhao, C., Ren, J., Qu, X., 2012. *Chem. Commun.* 48 (93), 11428–11430.
- Cunningham, T.F., Putterman, M.R., Desai, A., Horne, W.S., Saxena, S., 2015. *Angew. Chem. Int. Ed.* 54 (21), 6330–6334.
- Gandhiraman, R.P., Le, N.C.H., Dixit, C.K., Volcke, C., Doyle, C., Gubala, V., Uppal, S., Monaghan, R., James, B., O'Kennedy, R., Daniels, S., Williams, D.E., 2011. *ACS Appl. Mater. Interfaces* 3 (12), 4640–4648.
- Hassani, S., Akmal, M.R., Salek-Maghsoudi, A., Rahmani, S., Ganjali, M.R., Norouzi, P., Abdollahi, M., 2018. *Biosens. Bioelectron.* 120, 122–128.
- Kelnar, K., Peltier, H.J., Leatherbury, N., Stoudemire, J., Bader, A.G., 2014. *Anal. Chem.* 86 (3), 1534–1542.
- Ki, J., Jang, E., Han, S., Shin, M.K., Kang, B., Huh, Y.M., Haam, S., 2017. *ACS Appl. Mater. Interfaces* 9 (21), 17702–17709.
- Kobori, A., Horie, S., Suda, H., Saito, I., Nakatani, K., 2004. *J. Am. Chem. Soc.* 126 (2), 557–562.
- Li, B.L., Jiang, Y., Chen, X., Ellington, A.D., 2012. *J. Am. Chem. Soc.* 134 (34), 13918–13921.
- Li, H.Y., Chang, J.F., Gai, P.P., Li, F., 2018a. *ACS Appl. Mater. Interfaces* 10 (5), 4561–4568.
- Li, H.Y., Chang, J.F., Hou, T., Li, F., 2017a. *Anal. Chem.* 89 (1), 673–680.
- Li, H.Y., Wang, C.F., Hou, T., Li, F., 2017b. *Anal. Chem.* 89 (17), 9100–9107.
- Li, J., Liu, S., Sun, L., Li, W., Zhang, S.-Y., Yang, S., Li, J., Yang, H.-H., 2018b. *J. Am. Chem. Soc.* 140 (48), 16589–16595.
- Lin, Y., Chen, C., Wang, C., Pu, F., Ren, J., Qu, X., 2011a. *Chem. Commun.* 47 (4), 1181–1183.
- Lin, Y., Tao, Y., Ren, J., Pu, F., Qu, X., 2011b. *Biosens. Bioelectron.* 28 (1), 339–343.
- Liu, Q.Y., Yang, Y.T., Li, H., Zhu, R.R., Shao, Q., Yang, S.G., Xu, J.J., 2015. *Biosens. Bioelectron.* 64, 147–153.
- Liu, Q.Y., Yang, Y.T., Lv, X.T., Ding, Y.A., Zhang, Y.Z., Jing, J.J., Xu, C.X., 2017. *Sens. Actuators, B* 240, 726–734.
- Lou, Z., Han, H., Zhou, M., Wan, J., Sun, Q., Zhou, X., Gu, N., 2017. *Anal. Chem.* 89 (24), 13472–13479.
- Luo, Y.P., Zhang, L.M., Liu, W., Yu, Y.Y., Tian, Y., 2015. *Angew. Chem. Int. Ed.* 54 (47), 14053–14056.
- Ma, J.L., Yin, B.C., Wu, X., Ye, B.C., 2017. *Anal. Chem.* 89 (2), 1323–1328.
- Masud, M.K., Islam, M.N., Haque, M.H., Tanaka, S., Gopalan, V., Alici, G., Nguyen, N.T., Lam, A.K., Hossain, M.S.A., Yamauchi, Y., Shiddiky, M.J.A., 2017. *Chem. Commun.* 53 (58), 8231–8234.
- Mehrgardi, M.A., Ahangar, L.E., 2011. *Biosens. Bioelectron.* 26 (11), 4308–4313.
- Meng, X., Wang, H., Chen, N., Ding, P., Shi, H., Zhai, X., Su, Y., He, Y., 2018. *Anal. Chem.* 90 (9), 5646–5653.
- Mills, D.M., Martin, C.P., Armas, S.M., Calvo-Marzal, P., Kolpashchikov, D.M., Chumbimuni-Torres, K.Y., 2018. *Biosens. Bioelectron.* 109, 35–42.
- Nguyen, H.H., Park, J., Kang, S., Kim, M., 2015. *Sensors* 15 (5), 10481–10510.
- Ocsoy, I., Paret, M.L., Ocsoy, M.A., Kunwar, S., Chen, T., You, M.X., Tan, W.H., 2013. *ACS Nano* 7 (10), 8972–8980.
- Park, J., Yeo, J.S., 2014. *Chem. Commun.* 50 (11), 1366–1368.
- Plotnikova, A., Osipenko, A., Masevičius, V., Vilkaitis, G., Klimašauskas, S., 2014. *J. Am. Chem. Soc.* 136 (39), 13550–13553.
- Qian, S., Lin, M., Ji, W., Yuan, H., Zhang, Y., Jing, Z., Zhao, J., Masson, J.F., Peng, W., 2018. *ACS Sens.* 3 (5), 929–935.
- Tian, N., Zhou, Z.-Y., Yu, N.-F., Wang, L.-Y., Sun, S.-G., 2010. *J. Am. Chem. Soc.* 132 (22), 7580–7581.
- Wang, Q., Li, Q., Yang, X., Wang, K., Du, S., Zhang, H., Nie, Y., 2016. *Biosens. Bioelectron.* 77, 1001–1007.
- Wolf, L.K., Fullenkamp, D.E., Georgiadis, R.M., 2005. *J. Am. Chem. Soc.* 127 (49), 17453–17459.
- Xia, X., Hao, Y., Hu, S., Wang, J., 2014. *Biosens. Bioelectron.* 51, 36–39.
- Yan, H., Bhattarai, U., Guo, Z.-F., Liang, F.-S., 2017. *J. Am. Chem. Soc.* 139 (14), 4987–4990.
- Yang, C., Shi, K., Dou, B., Xiang, Y., Chai, Y., Yuan, R., 2015. *ACS Appl. Mater. Interfaces* 7 (2), 1188–1193.
- Yang, C.T., Pourhassan-Moghaddam, M., Wu, L., Bai, P., Thierry, B., 2017. *ACS Sens.* 2 (5), 635–640.
- Yao, G.H., Liang, R.P., Yu, X.D., Huang, C.F., Zhang, L., Qiu, J.D., 2015. *Anal. Chem.* 87 (2), 929–936.
- Zeng, S., Baillargeat, D., Ho, H.P., Yong, K.T., 2014. *Chem. Soc. Rev.* 43 (10), 3426–3452.
- Zhou, F., Yao, Y., Luo, J., Zhang, X., Zhang, Y., Yin, D., Gao, F., Wang, P., 2017b. *Anal. Chim. Acta* 969, 8–17.
- Zhou, L., Arugula, M.A., Chin, B.A., Simonian, A.L., 2018. *ACS Appl. Mater. Interfaces* 10 (48), 41763–41772.
- Zhou, Y., Chen, M., Zhuo, Y., Chai, Y., Xu, W., Yuan, R., 2017a. *Anal. Chem.* 89 (12), 6787–6793.
- Zubritsky, E., 2000. *Anal. Chem.* 72 (7), 289–292.